

1 **Modeling light-use efficiency in a subtropical mangrove forest equipped with CO<sub>2</sub> eddy covariance**

2

3 **J.G. Barr<sup>1</sup>, V. Engel<sup>2</sup>, J.D. Fuentes<sup>3</sup>, D.O. Fuller<sup>4</sup>, H. Kwon<sup>5</sup>**

4

5 <sup>1</sup>South Florida Natural Resource Center, Everglades National Park, Homestead, FL 33030

6

7 <sup>2</sup>Southeast Ecological Science Center, U.S. Geological Survey, Gainesville FL 32653

8

9 <sup>3</sup>Department of Meteorology, The Pennsylvania State University, University Park, PA 16802

10

11 <sup>4</sup>Department of Geography and Regional Studies, University of Miami, Coral Gables, FL 33124

12

13 <sup>5</sup>Department of Civil Engineering, Chonbuk National University, Jeonju, South Korea

14

15 Correspondence to: J.G. Barr (Jordan\_Barr@nps.gov)

16

17

18 **Abstract**

19 Despite the importance of mangrove ecosystems in the global carbon budget, the relationships between  
20 environmental drivers and carbon dynamics in these forests remain poorly understood. This limited  
21 understanding is partly a result of the challenges associated with *in situ* flux studies. Tower-based CO<sub>2</sub>  
22 eddy covariance (EC) systems are installed in only a few mangrove forests worldwide and the longest EC  
23 record from the Florida Everglades contains less than 9 years of observations. A primary goal of the  
24 present study was to develop a methodology to estimate canopy-scale photosynthetic light use efficiency  
25 in this forest. These tower-based observations represent a basis for associating CO<sub>2</sub> fluxes with canopy  
26 light use properties, and thus provide the means for utilizing satellite-based reflectance data for larger-  
27 scale investigations. We present a model for mangrove canopy light use efficiency utilizing the enhanced  
28 green vegetation index (EVI) derived from the Moderate Resolution Imaging Spectroradiometer (MODIS)  
29 that is capable of predicting changes in mangrove forest CO<sub>2</sub> fluxes caused by a hurricane disturbance  
30 and changes in regional environmental conditions, including temperature and salinity. Model parameters  
31 are solved for in a Bayesian framework. The model structure requires estimates of ecosystem respiration  
32 ( $R_E$ ), and we present the first-ever tower-based estimates of mangrove forest  $R_E$  derived from night-time  
33 CO<sub>2</sub> fluxes. Our investigation is also the first to show the effects of salinity on mangrove forest CO<sub>2</sub>  
34 uptake, which declines 5% per each 10 parts per thousand (ppt) increases in salinity. Light use efficiency  
35 in this forest declines with increasing daily photosynthetic active radiation, which is an important  
36 departure from the assumption of constant light use efficiency typically applied in satellite-driven models.  
37 The model developed here provides a framework for estimating CO<sub>2</sub> uptake by these forests from  
38 reflectance data and information about environmental conditions.

39

## 40 1 Introduction

41 Mangrove forests have received significant attention recently due to an increased recognition of the role  
42 these systems play in global carbon (C) cycles (Donato et al., 2011). However, compared to terrestrial  
43 systems, the processes that regulate ecosystem-atmosphere carbon dioxide (CO<sub>2</sub>) fluxes, including gross  
44 primary productivity (GPP) and ecosystem respiration (R<sub>E</sub>), are not well understood. Tower-based, eddy  
45 covariance (EC) measures of the net (i.e., GPP-R<sub>E</sub>) ecosystem-atmosphere CO<sub>2</sub> exchange (or NEE) in  
46 conjunction with continuous measurements of environmental variables were started only recently  
47 compared to terrestrial systems (see Barr et al., 2010) and remain extremely rare. These observations  
48 show that canopy-scale CO<sub>2</sub> fluxes are influenced by stressors that are unique to mangrove forests,  
49 including periodic flooding and variable soil pore-water salinity. Using these EC data to calculate canopy-  
50 level light use efficiency (LUE, defined as GPP divided by incoming photosynthetic active radiation (PAR))  
51 will improve our understanding of C cycling in these forests. Modeling canopy-level LUE in relation to  
52 PAR and ground-based scalars in turn provides a first step towards using satellite reflectance data to  
53 define the larger role these forests play in both regional and global C budgets. However, typical LUE  
54 models developed for terrestrial systems do not account for the unique factors that influence C dynamics  
55 in tidal forests, and new approaches are needed.

56 For all plant communities, including mangrove forests, the net ecosystem carbon balance (NECB, or  
57 the C accumulating in plants and soils (Chapin et al., 2006)) can be estimated using the following  
58 expression:

$$59 \text{NECB} = -\text{NEE} + F_{\text{DIC}} + F_{\text{DOC}} + F_{\text{POC}} \quad (1)$$

60 where F<sub>DIC</sub>, F<sub>DOC</sub>, and F<sub>POC</sub> are the net lateral exchanges of dissolved inorganic C (DIC), organic C  
61 (DOC), and particulate organic C (POC). All terms in equation (1) are expressed in g C m<sup>-2</sup> t<sup>-1</sup>. Negative  
62 NEE values represent a loss of C from the atmosphere, and negative F values represent C loss from the  
63 ecosystem. In terrestrial systems with minimal F, positive nighttime NEE values are considered a proxy  
64 for R<sub>E</sub>. Compared to terrestrial systems, mangrove forests are characterized by low nighttime NEE, large  
65 daytime -NEE values and large -F (Barr et al., 2012). However, comprehensive *in situ* measures of  
66 mangrove forest C dynamics that simultaneously account for both vertical C fluxes (i.e., NEE) and lateral  
67 C fluxes (F) have not been attempted. Continuous and long-term estimates of F<sub>DIC</sub>, F<sub>DOC</sub>, and F<sub>POC</sub>  
68 usually do not exist. Instead, lateral C fluxes are ordinarily determined only during short-term intensive  
69 field campaigns (e.g., Romigh et al., 2006; Alongi et al., 2004; Souza et al., 2009; Mayorga et al., 2005).  
70 In the absence of these measurements, nighttime, tower-based NEE estimates in many mangrove forests  
71 cannot be used as a direct proxy for R<sub>E</sub> as they are in terrestrial systems, since the actual ecosystem-  
72 scale respiratory CO<sub>2</sub> fluxes in tidal systems will also include respiratory fluxes derived from F transported  
73 outside of the EC footprint. Non-standard methods for calculating R<sub>E</sub> and, therefore, GPP are required in  
74 mangrove forests utilizing EC.

75 Monteith (1966, 1972) first proposed the concept of relating GPP to PAR through a light use  
76 efficiency term, ε, or multiplicative efficiency terms. Light use efficiencies describe the process of solar

77 irradiance transmission through the atmosphere, light absorption by green vegetation, and photosynthetic  
78 CO<sub>2</sub> assimilation by foliage. Light use efficiency terms in ecosystem models (e.g., Xiao et al., 2004; Cook  
79 et al., 2008; Potter, 2010) are calculated in a two-step process. First, functional relationships are  
80 established between environmental drivers, such as temperature and water stress that regulate  
81 physiological functioning and thus GPP. A second step is to determine how much of the incident solar  
82 irradiance is absorbed by photosynthetic active green vegetation. Useful proxies for the process of light  
83 absorption by vegetation can be determined using remote sensing information (Zhao and Running, 2008).  
84 In one of the first attempts to incorporate remote sensing information into ecosystem models, Tucker et al.  
85 (1983) estimated the productivity of grasslands using the normalized difference vegetation index (NDVI)  
86 from the Advanced Very High Resolution Radiometer (AVHRR) aboard polar orbiting platforms. Several  
87 other models have been tested and validated using relationships between remote sensing information  
88 and ground-based C flux data (Heinsch et al., 2006; Turner et al., 2006; Zhao et al., 2005). More recently,  
89 Chen et al. (2010) applied the enhanced vegetation index (EVI) as input into a vegetation photosynthesis  
90 model (VPM, Xiao et al., 2004) to take advantage of the high return frequency (1-2 per day) of the  
91 Moderate Resolution Imaging Spectroradiometer (MODIS) and the increased spatial resolution (30-m) of  
92 LANDSAT. However, the usefulness of satellite reflectance-driven models such as these developed for  
93 simulating terrestrial GPP, such as the MODIS GPP product  
94 (<http://modis.gsfc.nasa.gov/data/dataproduct/nontech/MOD17.php>) has not been determined for mangrove  
95 forests. These types of models are needed to better integrate estimates of mangrove forest CO<sub>2</sub>  
96 assimilation patterns across tropical and subtropical coastal zones into global-scale C balance  
97 calculations. Therefore, the objectives of this study are: 1) to calculate R<sub>E</sub> and GPP in a tidal mangrove  
98 forest using a novel application of EC-based estimates of NEE, 2) to parameterize and test a model of  
99 daily canopy GPP and LUE driven by satellite reflectance data, and 3) to compare these GPP estimates  
100 to the MODIS GPP product for this location.

101

## 102 **2 Methods**

### 103 **2.1 Site description and meteorological and eddy covariance measurements**

104 The study site (25.3646 °N, 81.0779 °W), located within Everglades National Park, is near the mouth of  
105 the Shark River and ~4 km from the Gulf of Mexico (Fig. 1). The onsite 30-m eddy covariance tower is  
106 co-located with long-term monitoring sites operated by the Florida Coastal Everglades Long Term  
107 Ecological Research (FCE LTER, site SRS6) program and the US Geological Survey (site SH3). Around  
108 the tower site, the dominant mangrove species include *Rhizophora mangle*, *Avicennia germinans*, and  
109 *Laguncularia racemosa*, and their maximum heights reach about 19 m. Meteorological measurements  
110 and EC observations to determine NEE have been made since 2003 at a height of 27 m.

111 During October 2005, the forest experienced a major disturbance caused by Hurricane Wilma. The  
112 disturbance caused major defoliation of the forest and tree mortality, with 25 % of stems >1.5 m in height  
113 being destroyed by the hurricane winds (Barr et al., 2012). Following Hurricane Wilma, instruments were

114 deployed on a new 30-m tower with renewed measurements beginning in November 2006 (Barr et al.,  
 115 2012). Continuous meteorological measurements are recorded as 1-minute averages on data loggers  
 116 (model CR3000, Campbell Scientific, Inc., Logan, UT), and stored in files saved at 30-min intervals in a  
 117 laptop computer located on site. High frequency (10 Hertz) EC data are stored directly on the laptop  
 118 computer for subsequent processing to derive 30-min average fluxes (using Matlab code, The  
 119 Mathworks, Inc., Natick, MA), following the protocols employed by scientists associated with the  
 120 AmeriFlux network (<http://public.ornl.gov/ameriflux/index.html>). Data gap-filling procedures were  
 121 implemented to produce continuous time series. Additional details for site characteristics and data  
 122 processing protocols are provided in Barr et al. (2010) and Barr et al. (2012).

123

## 124 **2.2 Partitioning NEE into $R_E$ and GPP**

125 Estimates of ecosystem respiration ( $R_E$ ;  $\mu\text{mol CO}_2 \text{ m}^{-2} \text{ s}^{-1}$ ) are needed to calculate GPP ( $\mu\text{mol CO}_2 \text{ m}^{-2} \text{ s}^{-1}$ ), which is defined as  $\text{GPP} = -\text{NEE} + R_E$ . In tidal mangrove forests equipped with EC, nighttime NEE can  
 126 be considered as a proxy for nighttime  $R_E$  only when the sediment surface is exposed to the atmosphere  
 127 during low tides. NEE represents the EC-derived  $\text{CO}_2$  flux at a height of 27 m plus the amount of  $\text{CO}_2$ ,  
 128 stored in column of air below this height since the previous time step. This storage was estimated from  
 129 the change in  $\text{CO}_2$  mixing ratio at the infrared gas analyzer level of 27 m (Barr et al., 2010). When the  
 130 sediment surface is inundated during a flood tide, a fraction of the  $\text{CO}_2$  respired by soil, roots, and detritus  
 131 is dissolved in the overlying water column and transported into the adjacent estuary as DIC during the  
 132 subsequent ebb tide. Therefore, tower-based nighttime  $\text{NEE} \neq R_E$  when the surface is inundated. To  
 133 correct for this effect in our calculations of GPP, non-linear least squares regression analyses were  
 134 performed to express nighttime  $R_E$  as a function of air temperature,  $T_A$  (after Reichstein et al., 2005) using  
 135 only valid NEE values determined when the sediment surface was exposed (Fig. 2). Regression  
 136 analyses of nighttime NEE as a function of  $T_A$  during high tides show significantly different relationships  
 137 than at low tide and are included in Fig. 2 for comparison. High tide data were excluded from our  
 138 calculations and the function relating low-tide  $R_E$  to  $T_A$  was used to gap-fill these periods. Data gaps  
 139 occurring when the EC system was not operating, or when there was insufficient turbulence and when the  
 140 flux footprint included large contributions from adjacent rivers (Barr et al., 2010) were also filled using this  
 141 function. The  $R_E$  function in (2) includes both an Arrhenius-type activation component and a high  
 142 temperature deactivation response.

$$144 \quad R_E = R_{E20} \exp\left(E_0 \left(\frac{1}{T_{\text{REF}} - T_0} - \frac{1}{T_A - T_0}\right)\right) / \left(1 + \exp(E_D(T_A - T_D))\right) \quad (2)$$

145 The  $R_{E20}$  ( $\mu\text{mol (CO}_2) \text{ m}^{-2} \text{ s}^{-1}$ ) represents the ecosystem-level respiration rate at the reference air  
 146 temperature,  $T_{\text{REF}}$ , which is set as 293.15 K. This  $R_{E20}$  value differs from the more common reference  
 147 temperature of 283.15 K (Lloyd and Taylor, 1994) because it is a closer approximation of the minimum  
 148 temperature range frequently observed in this forest. Also, the  $R_E$  was related to air temperature rather  
 149 than the more prevalently used soil temperature (Lloyd and Taylor, 1994). The use of air, rather than soil

150 temperature was justified by considering the sources contributing to  $R_E$ . Foliage respiration alone can  
 151 contribute 73% of the total  $R_E$  during low tide periods at night (Barr et al., 2010). Measurements of soil  
 152 respiration in relatively undisturbed mangrove forests throughout the Caribbean, Australia, and New  
 153 Zealand (Lovelock, 2008) suggest that soils contribute less respired  $CO_2$  to  $R_E$  compared to that of above  
 154 ground sources. However, the fractional contribution of the soil to  $R_E$  may increase as a result of  
 155 hurricanes or other disturbances. Soil respiration increased by 18% in a dry tropical forest in Mexico one  
 156 year following disturbance from Hurricane Wilma (Vargas and Allen, 2008).

157 In (2), the  $E_o$  (K) and  $E_D$  (K) parameters are temperature-dependent activation energy and  
 158 deactivation sensitivity, respectively. The  $T_o$  (K) also accounts for changes in activation energy  
 159 associated with variations in temperature. Its expected values range between 0 K and observed air  
 160 temperature (Lloyd and Taylor, 1994). The  $T_D$  (K) term is the temperature at which deactivation occurs,  
 161 and represents a unique feature in this study that explicitly accounts for a reduction in respiration above a  
 162 threshold temperature. The deactivation term, represented by the denominator in (2), has the same  
 163 functional response to high temperature (>35 C) as relationships describing foliage carboxylation and  
 164 dark respiration rates (Campbell and Norman, 1998). The response of  $R_E$  to temperature is a dynamic  
 165 process, and consequently the fitted characteristics in (2) are expected to change seasonally. To capture  
 166 such variability in respiratory responses, values of  $R_E$  and regression characteristics (e.g.,  $R_{E20}$ ,  $E_o$ ,  $T_o$ ,  
 167  $E_D$ ,  $T_D$ ) were determined for a 3-day moving window using nighttime data during low tide periods from a  
 168 15-day centered window. Similar to the findings of Reichstein et al. (2005), a window size of 15 days was  
 169 sufficiently long to provide adequate data and temperature range for performing the non-linear regression  
 170 of (2) and short enough to minimize the confounding seasonal changes in respiration response. During  
 171 each 3-day period, the relationship in (2) was used to compute half-hourly daytime  $R_E$ , and half-hourly  
 172 GPP values were computed as the difference between  $R_E$  and daytime NEE (i.e.,  $GPP = -NEE + R_E$ ). Half-  
 173 hourly values of GPP ( $\mu\text{mol C m}^{-2} \text{ s}^{-1}$ ) were summed as shown in (3) to provide daily GPP and 8-day  
 174 average values in units of  $\text{mol C m}^{-2}$  per day. This 8-day time step matches that of the MODIS product  
 175 and removes noise in the daily data while retaining seasonal trends. The coefficient of 0.0216 in (3)  
 176 converts units of  $\mu\text{mol CO}_2 \text{ m}^{-2} \text{ s}^{-1}$  to  $\text{g C m}^{-2}$  per each 30-min flux averaging interval.

177

$$178 \quad GPP = 0.0216 \sum_{i=1}^{48} GPP_{30\text{-min}} \quad (3)$$

179

### 180 **2.3 Albedo, EVI, and MODIS GPP**

181 We investigate seasonal changes in canopy structural properties using two measures of canopy  
 182 reflectance: albedo and EVI. The surface albedo (Fig. 3a) was estimated as the ratio of reflected to  
 183 incoming solar irradiance measured above the canopy. The adjusted albedo was estimated as the  
 184 average of albedo values for the periods when the solar elevation angle ranged between 35 and 50

185 degrees. This adjustment was necessary to remove the influence of changing daily solar elevation angles  
186 over the course of the study.

187 The MODIS EVI product was used to examine seasonal patterns in the mangrove canopy reflectance  
188 properties. It is well established (Huete et al., 2002; Jiang et al., 2008) that the EVI data are more reliable  
189 compared to NDVI in environments with high biomass content. For this study, the EVI data (Fig. 3b) were  
190 obtained from the MOD13A1 product (EOS; <http://modis.gsfc.nasa.gov/>). The mangrove flux tower site is  
191 included in grid h10v06, with a 500-m spatial resolution. Using GIS (Geographic Information System)  
192 software (Matlab Mapping Toolbox, The Mathworks, Inc., Natick, MA), the 16-day composite average EVI  
193 values for the pixel corresponding to the flux tower site and the 8 adjacent pixels were extracted for the  
194 period 2000 to 2011. This 9-pixel domain approximates the extent of the EC measurement footprint (see  
195 Fig. 1 in Barr et al., 2010). The MODIS GPP product, MOD17A2 ([https://lpdaac.usgs.gov](https://lpdaac.usgs.gov/)), was also  
196 extracted from grid h10v06 for comparison with estimated and modeled GPP in this study. MODIS GPP  
197 represents a 16-day composite average with a 1-km spatial resolution. Values were averaged for the  
198 pixel corresponding to flux tower site and 4 adjacent pixels included within the measurement footprint and  
199 not centered over water.

200

#### 201 **2.4 LUE modeling framework**

202 The mangrove vegetation photosynthesis light-use efficiency model (MVP-LUE) presented here is based  
203 on the production efficiency modeling (PEM) framework (Prince and Goward, 1995; Running et al., 1999;  
204 Running et al., 2000). It has the basic form of

205

$$206 \quad LUE = \sum GPP / \sum PAR = \varepsilon_g \times fPAR \quad (4)$$

207 where LUE (mol C (mol photons)<sup>-1</sup>) is calculated as the ratio of 8-day sums of GPP to PAR (mol (photons)  
208 m<sup>-2</sup>). The  $\varepsilon_g$  is a quantum efficiency (mol C (mol photons)<sup>-1</sup>) that describes conversion of incident PAR  
209 into gross primary production specific to the irradiance incident on green vegetation. fPAR (unitless) is  
210 the ratio (8-day average) of PAR absorbed by green vegetation to total incident PAR determined above  
211 the vegetated landscape. Previous modeling studies suggested that fPAR linearly increased with EVI  
212 (Xiao et al., 2004) or NDVI (Goetz et al., 1999; Schubert et al., 2010). However, in the present study,  
213 fPAR increases in response to increasing EVI as determined from the 500-m spatial resolution data  
214 according to:

$$215 \quad fPAR = 1 - e^{-m_{EVI} \times EVI} \quad (5)$$

216 where  $m_{EVI}$  determines the initial slope of fPAR response to increasing EVI. The rate of increase in 8-day  
217 average fPAR to increasing EVI diminishes and is dependent on the value of  $m_{EVI}$ . We found that the  
218 observed quantum LUE of the mangrove ecosystem approaches some optimum efficiency,  $\varepsilon_0$  (defined as  
219 the light conditions when maximum NEE is attained). The  $\varepsilon_0$  is not known *a priori* and must be determined  
220 from an optimization procedure. Most of the time, environmental conditions are less than optimal, and

221 therefore  $\varepsilon_g$  is often less than  $\varepsilon_0$ . The  $\varepsilon_g$  represents a multiplicative chain of efficiencies (Monteith, 1972)  
 222 where each  $f$  term in the chain accounts for a reduction in quantum LUE below  $\varepsilon_0$ .

223 Several variables contribute to reducing the quantum efficiency in this forest. The first is elevated  
 224 foliage temperature resulting from air temperatures ( $T_A > 303$  K) which elicit sub-optimal carboxylation  
 225 rates (Barr et al., 2010). Such responses to elevated temperature can be expressed by the relationship  
 226 shown in (6) formulated by Raich et al. (1991):

$$227 \quad f_{T_A} = \frac{(T_A - T_{Min})(T_A - T_{Max})}{[(T_A - T_{Min})(T_A - T_{Max})] - (T_A - T_{Opt})^2} \quad (6)$$

228 where  $T_A$  is air temperature recorded at 27 m above the ground (Fig. 4a), and  $T_{Min}$ ,  $T_{Max}$ , and  $T_{Opt}$  are  
 229 minimum, maximum, and optimal temperatures for GPP, respectively. The function  $f_{T_A}$  attains the value  
 230 of 1 when  $T_A$  becomes the same as  $T_{Opt}$  and is set to zero for  $T_A < T_{Min}$ . Raich et al. (1991) determined  
 231 GPP as a function of temperature for several vegetation types in South America, including tropical  
 232 evergreen forests, grasslands, and temperate forests. To compare the temperature dependency of  
 233 productivity that occurred independently of the magnitude of GPP, ratios of GPP to site-specific maximum  
 234 GPP ( $GPP_{Max}$ ) were compared. All three vegetation types exhibited ratios (i.e.,  $GPP/GPP_{Max}$ ) that  
 235 followed the relationship in (6) but each possessed its own unique characteristics ( $T_{Min}$ ,  $T_{Max}$ , and  $T_{Opt}$ ).  
 236 While this relationship in (6) was not previously quantified for the mangrove ecosystem, the shape of the  
 237 curve is consistent with  $-NEE$  response to  $T_A$  during 2004-2005 (see Fig. 6 in Barr et al., 2010) for  
 238 conditions when  $PAR > 1000 \mu\text{mol (photons) m}^{-2} \text{ s}^{-1}$ .

239 Barr et al. (2010) showed a linear decline in the 8-day averages of  $LUE/LUE_{salinity=0}$  versus 8-day  
 240 average soil pore salinity between 10-40 parts per thousand (ppt) of dissolved solutes during both pre  
 241 (2004-2005) and post-hurricane (November 2006 to December 2011) periods. This reduction in LUE  
 242 attributed to changes in salinity ( $f_{sal}$ ) is defined in (7).  $LUE_{salinity=0}$  was determined from the intercept of the  
 243 regression.

$$244 \quad f_{sal} = 1 - m_{sal} \times salinity \quad (7)$$

245 The  $m_{sal}$  defines the rate of decrease in  $f_{sal}$  in response to increasing salinity. The decline in LUE with  
 246 increasing salinity may be partially attributed to photosynthetic saturation under high PAR ( $>50$  mol  
 247 photons  $\text{m}^{-2} \text{ day}^{-1}$ ) which coincides with maximal salinity during May and June. A linear function in (8) was  
 248 included to account for photosynthesis saturation manifested as declining LUE with increasing PAR.

$$249 \quad f_{PAR} = 1 - m_{PAR} \times PAR \quad (8)$$

250 The  $m_{PAR}$  defines the rate of decrease in  $f_{PAR}$  in response to increasing PAR.

251 Since  $f_{PAR}$ ,  $f_{T_A}$ ,  $f_{sal}$ , and  $f_{PAR}$  have a maximum value of 1, light-use efficiencies approach  $\varepsilon_0$  as EVI  
 252 attains the value of 1, air temperature approaches  $T_{Opt}$ , and salinity (ppt) and PAR (mol photons  $\text{m}^{-2} \text{ day}^{-1}$ )  
 253 decrease to zero. The overall resulting quantum efficiency may then be expressed as the multiplicative  
 254 set of efficiencies to account for the effects of temperature, salinity, and PAR as shown in (9).

$$\varepsilon_g = \varepsilon_0 \times f_{T_A} \times f_{sal} \times f_{PAR} \quad (9)$$

To implement the model described in (4) to (9), the individual forcing terms (i.e.,  $\varepsilon_0$ ,  $m_{EVI}$ ,  $T_{Min}$ ,  $T_{Max}$ ,  $T_{Opt}$ ,  $m_{sal}$ ,  $m_{PAR}$ ) must be derived from the data through the use of an optimization approach. We apply a Bayesian framework to solve for the posterior probability of model parameters and LUE during the periods 2004-2005 and November 2006 to 2011 when EC-derived estimates of GPP and LUE are available. The Bayesian analytical framework provides several advantages over more traditional model optimization approaches, including the ability to directly estimate uncertainties in modeled LUE without the use of *ad hoc* procedures. Outputs from the optimization procedure provide the forcing terms (e.g.,  $m_{EVI}$ ,  $T_{Opt}$ , etc.) that are described probabilistically, thereby allowing us to assess the applicability of each term. To cast this model within the Bayesian framework, LUE was considered to exhibit a normal distribution as:

$$LUE \sim N(\mu_{LUE}, \sigma_{LUE}) \quad (10)$$

where  $\mu_{LUE}$  is the time-varying mean and is equal to the expected 8-day average LUE with variance  $\sigma_{LUE}$ . A quantile-quantile (QQ) plot of LUE data against the standard normal distribution was used to verify the normality assumption. The forcing terms were considered to have a prior probability distribution which, when taken together, follow a multivariate normal distribution. That is,

$$\begin{pmatrix} \varepsilon_0 \\ m_{EVI} \\ T_{min} \\ T_{max} \\ T_{opt} \\ m_{sal} \\ m_{PAR} \end{pmatrix} \sim N \left( \begin{pmatrix} \mu_{\varepsilon_0} \\ \mu_{m_{EVI}} \\ \mu_{T_{min}} \\ \mu_{T_{max}} \\ \mu_{T_{opt}} \\ \mu_{m_{sal}} \\ \mu_{m_{PAR}} \end{pmatrix}, \Sigma \right) \quad (11)$$

with mean values,  $\mu$ , and covariance matrix,  $\Sigma$ . Off diagonal terms in  $\Sigma$  explicitly quantify the interdependence of model forcing terms, if such relationships exist. The inverse-Wishart distribution (O'Hagan and Forster, 2004) was used to describe the prior probability distribution of  $\Sigma$  because it represents the conjugate probability distribution of the multivariate normal distribution (Gelman et al., 2004), and expresses the uncertainty about  $\Sigma$  before the data are taken into account. The inverse-Wishart distribution represents the multivariate generalization of the scaled inverse-chi-squared distribution, which is the conjugate prior of the univariate normal distribution with unknown mean and variance. The inverse-Wishart distribution is defined by its own set of parameters,  $\Omega$  and  $\nu$ , commonly referred to as hyperparameters that represent the inverse scale matrix and degrees of freedom of the distribution, respectively.

$$\Sigma \sim Inv - Wishart(\Omega, \nu) \quad (12)$$

The  $\Omega$  was initialized with a 6 X 6 identity matrix, and the degrees of freedom,  $\nu = 6$ , representing the number of forcing terms. To learn the optimal probability distributions of the forcing terms ( $\varepsilon_0$ ,  $m_{EVI}$ ,  $T_{Min}$ ,  $T_{Max}$ ,  $T_{Opt}$ ,  $m_{sal}$ ), a Markov chain Monte Carlo (MCMC) procedure with Gibbs sampling (Cassella and George, 1992; Gilks et al., 1995) was performed in Matbugs. Matbugs is a Matlab (The Mathworks Inc.,

287 Natick, MA) interface to WinBUGS (Spiegelhalter et al., 2003). Gibbs sampling is the simplest of the  
288 Markov chain simulation algorithms (Gelman et al., 2004) and is used to directly sample from each  
289 conditional posterior distribution in a model. The resulting distribution of the forcing terms maximizes the  
290 likelihood that the LUE during the study period would be observed given the modeled LUE values. The  
291 Gibbs sampling procedure within WinBUGS requires initial values (i.e., best guesses) for all the forcing  
292 terms. Here, initial values were determined using a constrained optimization technique (Matlab  
293 Optimization Toolbox) in minimizing the sum of squared errors (SSE) between modeled and EC  
294 estimated 8-day LUE values obtained during the entire study period of 2004-2005 and November 2006 to  
295 December 2011. The constrained optimization is useful for obtaining a single point estimate of forcing  
296 terms, but does not provide a robust fit that includes the probability distribution of both parameters and  
297 modeled LUE values.

### 298 **3 Results and discussion**

#### 299 **3.1 Calculating $R_E$ and GPP from NEE**

300 Temperature, level of inundation, and foliage physiology drive respiration in this forest. Nighttime NEE  
301 increased with increasing  $T_A$  below  $\sim 25$  C during both high and low tide periods during 2004-2005 (Fig.  
302 2a). NEE was  $\sim 1 \mu\text{mol} (\text{CO}_2) \text{m}^{-2} \text{s}^{-1}$  higher during low tides, and NEE rates converged at temperatures  $>$   
303 25 C for both low and high tide periods during 2004-2005 and 2006-2011 (Fig. 2a and 2b, respectively).  
304 The exponential function with deactivation in (2) generally fit the NEE data during 2004-2005 and 2006-  
305 2011 periods (Fig. 2a-d). During 2004-2005, there was some evidence of bi-modality in  $R_E$  response to  
306 temperature with maxima occurring at  $T_A$  values ranging between 15 and 20 C and 25 to 28 C (Fig. 2a).  
307 The NEE was  $\sim 1 \mu\text{mol} (\text{CO}_2) \text{m}^{-2} \text{s}^{-1}$  higher during 2006-2011 compared to 2004-2005 for temperatures  
308 above 25 C, possibly due to an increased respiratory contribution from decomposing coarse woody debris  
309 (CWD) generated by the hurricane. The hurricane disturbance also resulted in warmer soils during 2006-  
310 2011 as more solar irradiance reached the soil surface beneath the damaged canopy (Barr et al., 2012).  
311 Such processes contributed to increased nighttime soil-air temperature gradients of 1 to 3 °C one year  
312 following disturbance (Table 1, Barr et al., 2012). Warmer soils in this system are expected to lead to  
313 increased belowground respiration and fractional increases in the belowground contribution to total  
314 nighttime  $R_E$ . During both pre- and post-disturbance periods, the functional response of  $R_E$  to air  
315 temperature exhibited a better fit than that using soil temperature.

316 The substantial seasonal changes in the respiratory response of the mangrove ecosystem (Fig. 2c,d)  
317 required the use of moving windows to fit (2) to these data. By partitioning the data by time, particularly  
318 into dry and wet season periods, the apparent bi-modality of nighttime NEE versus  $T_A$  response (Fig. 2a)  
319 was no longer apparent in the fitted model. The deactivation term in (2) that is needed to account for the  
320 observed decline in nighttime NEE at elevated  $T_A$  represents a unique characteristic of NEE patterns at  
321 this site compared to terrestrial forests. The temperature that defines the transition from increasing to  
322 decreasing respiratory response changed with seasons and as a result of disturbance. The increase in  
323 nighttime NEE in response to increasing  $T_A$  following the hurricane disturbance was most evident during

324 dry season months when the values increased by  $\sim 1 \mu\text{mol} (\text{CO}_2) \text{ m}^{-2} \text{ s}^{-1}$  as  $T_A$  exceeded 20 C, and  
325 continued on an upward trend until reaching a maximum of  $\sim 4 \mu\text{mol} (\text{CO}_2) \text{ m}^{-2} \text{ s}^{-1}$  at 22 C. Before the  
326 hurricane disturbance, NEE declined with temperatures exceeding 19 C. This increase in temperature,  
327 which defines peak respiratory response, also suggested an increased contribution of belowground  
328 respiration to  $R_E$  following disturbance. Quantifying the belowground contribution to  $R_E$  and the  
329 respiratory response to soil temperature require continuous measurements of belowground respiration,  
330 and such measurements were not made during this study. Due to the long-term nature of this  
331 investigation (spanning several years), the ecosystem respiration response captured the broad  
332 temperature ranges and levels of inundation experienced by the mangrove forest. As a result, it was  
333 possible to identify and quantify the dynamic character of the total respiratory responses,  $R_E$  to air  
334 temperature and subsequent declines in respiration above  $T_{\text{opt}}$ .

335

### 336 **3.2 Albedo and EVI**

337 Canopy-scale  $\text{CO}_2$  fluxes in mangrove forests vary seasonally as a result of changes in leaf area index  
338 and physiological responses to stressors. Such changes in the amount and function of foliage were  
339 inferred from temporal patterns in locally-measured surface albedo and the satellite-based greenness  
340 index, EVI. Albedo (Fig. 3a) varied seasonally with minimum values of 0.10 to 0.11 during May and June  
341 and maximum values of 0.13 to 0.15 during December to January. Albedo was about 0.12 during  
342 January 2007 and represented a decline of  $>0.01$  compared to values observed before Hurricane Wilma.  
343 Raw and adjusted albedo variability resulted in response to the recovery of foliage from the 2005  
344 disturbance, with apparent full recovery observed by 2011. Structural damage and defoliation of the  
345 mangrove forest was evident in the 16-day EVI time series (Fig. 3b) in the days following hurricane  
346 disturbance on October 24, 2005. The EVI declined from 0.4-0.5 to 0.22 following the 2005 disturbance.  
347 When tower measurements resumed in November 2006, re-foliation of surviving branches in upper  
348 canopy and new shoots in the understory had already occurred, with rapid re-growth occurring during  
349 June to October 2006. Yet, recovery was incomplete. EVI exhibited a decline of  $\sim 12\%$  when 2007-2008  
350 values were compared with those obtained in 2004-2005. These patterns were consistent with the 30%  
351 lower annual  $-NEE$  obtained for 2007. Though noisy, EVI exhibited similar sinusoidal seasonal patterns  
352 with maxima and minima values coinciding with the winter and summer solstices, respectively. EVI values  
353 represent a much larger area than do the albedo measurements ( $\sim 250,000 \text{ m}^2$  (per pixel), versus  $\sim 3000$   
354  $\text{m}^2$ , respectively). Such seasonal patterns were consistent with coherent patterns in monthly litter fall  
355 rates (Castaneda, 2010) within the flux footprint of the tower site.

356

### 357 **3.3 Physical drivers of mangrove productivity**

358 In south Florida, mangroves receive highly variable amounts of PAR (Fig. 4a) resulting from sinusoidal  
359 seasonal patterns and cloud cover from localized convective storms during the May to October wet  
360 season. The seasonal peak in PAR, and therefore the amount of energy available to drive

361 photosynthesis and GPP, occurred during April and May before the onset of the wet season in late May  
362 and June. Air temperatures (Fig. 4b) during March to May were between 25 and 30 C, and these  
363 conditions favored near optimal foliage carboxylation rates and GPP. However, surface water salinities  
364 (Fig. 4c) achieved their highest values (30-40 ppt) during this time period with peak values of 35-40 ppt  
365 extending into June and the start of the wet season. Such high salinities have previously been shown to  
366 contribute to reduced stomatal conductance and lowered net carbon assimilation at the leaf level (Barr et  
367 al., 2009) during the afternoon. Surface water salinities above 28 ppt also result in reduced NEE at the  
368 ecosystem scale (Barr et al., 2010). PAR declined throughout the wet season following the summer  
369 solstice in June coincident with reduced salinity levels resulting from increased freshwater flow through  
370 Shark River. Seasonal minima in salinity of 15-20 ppt occurred at the end of the wet season in October  
371 and November. Productivity was predicted to be seasonally lowest during December and January when  
372 air temperatures were below 20 C and when PAR reached seasonal minima of 20-30 mol photons m<sup>-2</sup> per  
373 day coincident with the winter solstice. During the extended cold spell of January 2010, temperatures  
374 reached nearly the freezing point during several early morning periods, with an 8-day average of  
375 approximately 10 C. Premature abscission of leaves in the canopy crown was observed on site, and  
376 likely resulted in reduced productivity and GPP.

377

### 378 **3.4 Canopy-scale CO<sub>2</sub> fluxes**

379 During the year-round growing season, this forest exhibited pronounced seasonal NEE patterns.  
380 Seasonal maxima in daily CO<sub>2</sub> uptake by the forest were observed during March to May in 2004-2005  
381 (Fig. 5a). Secondary peaks were observed during the month of November both before and after the  
382 hurricane. R<sub>E</sub> values (Fig. 5b) were seasonally highest during June to August with 8-day averages of  
383 0.30-0.40 and 0.30-0.55 mol C m<sup>-2</sup> day<sup>-1</sup> during 2004-2005 and 2007-2011, respectively. R<sub>E</sub> values  
384 were lowest between December and April. GPP (Fig. 5c) values were lowest during January and  
385 February coincident with seasonal minima in PAR and T<sub>A</sub>, and exhibited broad seasonal maxima between  
386 April and October, with values of 0.50-0.63 and 0.50-0.75 mol C m<sup>-2</sup> day<sup>-1</sup> during 2004-2005 and 2007-  
387 2011, respectively. LUE and PAR exhibited a strong negative correlation (R<sup>2</sup> = -0.70), suggesting that  
388 this ecosystem has adapted a physiological strategy for maintaining high GPP rates throughout most of  
389 the year. Elevated GPP values during cloudy days may be caused by higher fractions of diffuse  
390 compared to direct solar irradiance penetrating to lower canopy layers and raising the whole canopy LUE  
391 (Barr et al., 2010). Other forests experience enhanced C assimilation when subject to elevated diffuse  
392 irradiance (Gu et al., 2003).

393

### 394 **3.5 Light use efficiency**

395 Seasonal LUE patterns (Fig. 5d) were different compared to GPP and exhibited seasonal maxima (13-20  
396 mmol C (mol PAR)<sup>-1</sup>) during the months of September to December while PAR and salinity levels were  
397 declining or at their seasonal minima. LUE values generally declined with the progression of the dry

398 seasons, reaching annual minima of 7-10 mmol C (mol PAR)<sup>-1</sup> during the months of April to June, with  
399 some inter-annual variability. For example, in January 2010 LUE declined from an 8-day average of 19 to  
400 6 mmol C (mol PAR)<sup>-1</sup> from 19 December 2009 to 4 January 2010. This period coincided with several  
401 weeks of nighttime temperatures that approached 0 deg. C. These cold air masses induced foliage  
402 senescence and extensive litterfall. Salinity represents an important control on mangrove forest LUE, and  
403 therefore on ecosystem productivity. The regression analyses that relate the 8-day average LUE (i.e.  
404 LUE/LUE<sub>salinity=0</sub>) to salinity (Fig. 6) provided a 1.5% reduction in this ratio for every 1 ppt salinity increase.  
405 The trend formed the basis of the linear forcing of salinity on LUE included in relationship (7) which was  
406 required in the MVP-LUE model. The linear forcing was also consistent with previous results (Barr et al.,  
407 2010) and showed that midday LUE declined linearly with increasing salinity resulting in a 48% reduction  
408 in LUE from the lowest (16.7 ppt) to highest (34.7 ppt) salinity recorded during the 2004-2005 study  
409 period. The observed reductions in LUE were also consistent with previous studies (Ball and Pidsley,  
410 1995; Sobrado, 1999; Krauss and Allen, 2003; Parida et al., 2004) that indicated declines in leaf-level C  
411 assimilation in response to increasing soil water salinity. By extrapolating the observed linear decline in  
412 LUE, the productivity of the mangrove ecosystem ceases at surface water salinity approaching 70 ppt  
413 according to the model expressed in relationship (7). Whereas such high salinity levels do not occur at  
414 the Everglades study site, this estimate is in close agreement with average salinity tolerances of 60-90  
415 ppt reported for red, white, and black mangroves (Odum et al., 1982).

416

### 417 **3.6 MVP-LUE model results**

418 The cross-validated LUE model (Section 2.4) was capable of reproducing the observed responses of LUE  
419 and GPP to seasonal changes in environmental variables and recovery from a major hurricane  
420 disturbance. The modeled LUE median and 95% uncertainty bounds (Fig. 7) provided posterior  
421 predictions from 10,000 MCMC iterations in each of 3 independent chains determined from 5-fold cross  
422 validation. The largest discrepancies between estimated and modeled LUE occurred during March to  
423 May of 2007 and 2008 when estimated LUE were seasonally lowest. Posterior means calculated over  
424 the full 2004-2011 period of record were evaluated by the Pearson's correlation coefficient (R), the  
425 coefficient of efficiency (CoE), and the normalized bias (NB). The model performed nearly as well during  
426 validation ( $R^2 = 0.646$ , CoE = 0.645; NB = -0.015) as during training ( $R^2 = 0.651$ , CoE = 0.651; NB = -  
427 0.015).

428 Posterior distributions of model forcings (Table 1) allowed estimates of mangrove productivity in  
429 response to key forcings, including EVI, air temperature, and salinity. The positive  $m_{EVI}$  ( $4.03 \pm 0.52$ ;  
430 mean  $\pm 1$  s.d.) confirmed that fPAR, and therefore LUE, increased with EVI values. Air temperatures of  
431  $27.8 \pm 0.3$  C (mean  $\pm 1$  s.d.) favored optimal mangrove LUE. These temperatures (Fig. 4b) occurred most  
432 frequently during March to May and October to November. Both modeled and estimated LUE values  
433 declined as air temperatures approached the  $T_{Max}$  value of  $33.5 \pm 0.6$  C. The slope,  $m_{sal}$  ( $0.0047 \pm 0.0022$ )  
434 of the salinity forcing,  $f_{sal}$ , was a factor of three lower compared to the slope (0.0146) determined from the

435 response of  $LUE/LUE_{\text{salinity}=0}$  to salinity (Fig. 6). This apparent sharper decline in LUE with increasing  
436 salinity masked the effect of increasing PAR on LUE since seasonal PAR peaks in nearly the same  
437 season (May-June) as salinity. The Bayesian model results suggest that LUE significantly declined with  
438 increasing PAR with a slope,  $m_{\text{PAR}}$  of  $0.0101 \pm 0.0004$  (Table 1). Photosynthetic saturation with increasing  
439 PAR is currently not included in many light-use efficiency based models of productivity using satellite data  
440 (e.g., Xiao et al., 2004; Cook, et al., 2008; Chen et al., 2010). An increase from the lowest (15 ppt) to  
441 highest (39 ppt) salinity values observed during the study period was predicted to result in an 11%  
442 reduction in LUE. Also, an increase in PAR from the lowest ( $17 \text{ mol photons m}^{-2} \text{ day}^{-1}$ ) to highest ( $67 \text{ mol}$   
443  $\text{photons m}^{-2} \text{ day}^{-1}$ ) 8-day average during 2004-2011 resulted in a 51% reduction in LUE.

444 Air temperature, salinity, PAR, and EVI were all determined as significant predictors of LUE (Fig. 7).  
445 Low temperatures ( $\sim 10 \text{ C}$ ) during passages of cold fronts can last from a few days to weeks during  
446 December to February, resulting in large reductions in LUE and therefore GPP. For instance, the  
447 passage of cold fronts during January 2010 resulted in estimated and modeled LUE of  $\sim 6 \text{ mmol C (mol}$   
448  $\text{photons})^{-1}$ . While other controls on LUE remained constant, a change in air temperature from  $28 \text{ C}$   
449 (optimum temperature) to  $10 \text{ C}$  was predicted to result in a 65% reduction in LUE. These results confirm  
450 that mangrove forests become severely stressed when daily average temperatures drop below  $\sim 5 \text{ C}$ .  
451 Ross et al. (2009) measured high mangrove mortality following freeze events and the inability of  
452 mangroves to survive in climates where temperatures near the freezing point are frequent.

453

### 454 **3.7 MVP-LUE and MODIS GPP compared to EC GPP estimates**

455 The calibrated MVP-LUE model provided an improved mechanistic understanding of mangrove forest  
456 productivity compared to the standard MODIS GPP product. Specifically, least squares linear regressions  
457 of 8-day MVP-LUE modeled GPP values to EC-estimated GPP (Fig. 8a) indicated improved performance  
458 during 2004-2005 (slope = 0.720, intercept = 0.144,  $R^2 = 0.56$ ) compared to the 2006-2011 period  
459 following hurricane disturbance (slope = 0.483, intercept = 0.249,  $R^2 = 0.45$ ). The regression of MODIS  
460 GPP to EC-estimated GPP (Fig. 8b) suggested that the un-calibrated MODIS model only weakly captured  
461 productivity trends during 2004-2005 (slope = 0.477, intercept = 0.238,  $R^2 = 0.050$ ) and failed to capture  
462 any trends in GPP during 2006-2011 (slope = -0.372, intercept = 0.597,  $R^2 = 0.056$ ). The MVP-LUE  
463 model captured the broad seasonal maxima ( $0.5\text{-}0.7 \text{ mol C m}^{-2} \text{ day}^{-1}$ ) in EC-estimated GPP (Fig. 9) as a  
464 result of the strong dependence of mangrove forest productivity on air temperature. During December to  
465 February temperatures below  $\sim 20 \text{ C}$ , and to a lesser extent, shorter day length and daily PAR resulted in  
466 short-lived minima in GPP of  $0.2\text{-}0.35 \text{ mol C m}^{-2} \text{ day}^{-1}$ . The productivity response of mangrove forests to  
467 temperature has not been calibrated in the MODIS product and may partially explain the lack of  
468 correlation between MODIS GPP and EC-estimates. Also, the increased variance in MODIS GPP  
469 compared to EC-estimates (Fig. 8b) may be attributed to the MODIS model structure, which considers  
470 GPP as linearly increasing with PAR. The dampened GPP response to PAR identified in the MVP-LUE  
471 model resulted in seasonal variability in GPP better matching observations. Also, the MVP-LUE model

472 captured the sustained plateau in EC-estimated GPP into November. This resulted from lowered salinity  
473 stress during September to November represented in the model (eq. 7) and a modulated response of  
474 GPP to daily PAR integrals represented by the decline in LUE with increasing PAR (eq. 8).

475

#### 476 **4 Summary and conclusions**

477 This research represents a first attempt to design and verify a light use efficiency model for mangroves  
478 through the integration of remotely sensed information, and meteorological and hydrologic data. This  
479 study is the first one to quantify the respiratory responses of mangrove forests over temporal scales of  
480 several growing seasons. Ecosystem respiration was successfully modeled using an atypical response  
481 function that includes a high temperature (~33 C) deactivation term. Estimation of the temporally and  
482 temperature-dependent response of ecosystem respiration to air temperature provided a critical first step  
483 in modeling mangrove GPP.

484 Observed seasonal patterns in 8-day LUE were controlled by variability in daily PAR and air  
485 temperature, and to a lesser extent salinity and EVI fluctuations. LUE was lower when seasonal PAR  
486 was highest during April and May as a result of photosynthetic saturation. Also, salinity maxima of 35 to  
487 40 ppt contributed to canopy-scale reductions in LUE during April to early June amounting to a 5%  
488 reduction in LUE per each 10 ppt increase in salinity. Lowered LUE values during December and  
489 January were the result of lower air temperatures and lowered physiological activity. As temperatures  
490 approach 3 C, our model predicts that CO<sub>2</sub> uptake in these forests approaches zero. Significantly  
491 reduced EVI values after Hurricane Wilma in 2005 also resulted in significantly lowered model estimates  
492 of CO<sub>2</sub> uptake during the period when the EC tower was not operating. These results suggest that  
493 mangrove forest LUE can be quite variable in subtropical environments that experience seasonal  
494 variations in solar irradiance and air temperature, and disturbance from tropical storms.

495 The model and functional relationships determined in this study provide an important first step for  
496 understanding the larger role mangrove forests play in both regional and global C budgets. Remote  
497 sensing applications building on these results provide a means to estimate CO<sub>2</sub> fluxes in areas outside  
498 the flux tower footprint and in other mangrove forests around the tropics and subtropics. To do this,  
499 spatiotemporal patterns in salinity are required as model input, which may be resolved as in the  
500 Everglades from networks of hydrologic monitoring stations. PAR and air temperature data fields are also  
501 required. However, validating this model in locations not equipped with EC will require novel approaches  
502 that link predicted GPP values to other measurable parameters, such as biomass accumulation, or NECB  
503 at appropriate time scales. As more EC towers are deployed in other types of mangrove forests, LUE  
504 models such as this one may be used to identify patterns in quantum efficiencies across species, across  
505 forest structural characteristics (e.g. scattered or dwarf forests), and latitudinal position. The integrated  
506 datasets in turn will enable more precise approximations of the role mangrove forests play in global C  
507 dynamics.

508

509 **Acknowledgements**

510 J.D.F. and V.E. acknowledge support from the DOE (grant DE-FC02-06ER64298) to participate in this  
511 research. This research is also based upon work supported by the National Science Foundation through  
512 the Florida Coastal Everglades Long-Term Ecological Research program under grant number DBI-  
513 0620409. D.F. received support from NASA (Cooperative Agreement No.NNX08BA43A, WaterSCAPES:  
514 Science of Coupled Aquatic Processes in Ecosystems from Space). Any use of trade, product, or firm  
515 names is for descriptive purposes only and does not imply endorsement by the U.S. Government.

516

517

518 **References**

- 519 Alongi, D.M., Sasekumar, A., Chong, V.C., Pfizner, J., Trott, L.A., Tirendi, F., Dixon, P., Brunskill, G.J.:  
520 Sediment accumulation and organic material flux in a managed mangrove ecosystem: estimates of  
521 land-ocean-atmosphere exchange in peninsular Malaysia, *Mar. Geol.*, 208, 383-402, 2004.
- 522 Ball, M.C., Pidsley, S.M.: Growth responses to salinity in relation to distribution of two mangrove species,  
523 *Sonneratia alba* and *S. lanceolata*, in northern Australia, *Funct. Ecol.*, 9, 77-85, 1995.
- 524 Barr, J. G., Engel, V., Fuentes, J. D., Zieman, J. C., O'Halloran, T. L., Smith, T. J., and Anderson, G. H.:  
525 Controls on mangrove forest-atmosphere carbon dioxide exchanges in western Everglades National  
526 Park. *J. Geophys. Res. Biogeo.*, 115, 1-14, doi:10.1029/2009JG001186, 2010.
- 527 Barr, J.G., Engel, V., Smith, T.J., and Fuentes, J.D.: Hurricane disturbance and recovery of energy  
528 balance, CO<sub>2</sub> fluxes and canopy structure in a mangrove forest of the Florida Everglades. *Agr. Forest*  
529 *Meteorol.*, 153, 54-66, doi:10.1016/j.agrformet.2011.07.022, 2012.
- 530 Campbell, G.S., and Norman J.M.: *An Introduction to Environmental Biophysics – 2<sup>nd</sup> ed.*, Springer, New  
531 York, 286 pp., 1998.
- 532 Casella, G., and George, E.I.: Explaining the Gibbs sampler. *Am. Stat.*, 46(3), 167-174, 1992.
- 533 Castaneda, E.: Landscape patterns of community structure, biomass, and net primary productivity of  
534 mangrove forests in the Florida Coastal Everglades as a function of resources, regulators,  
535 hydroperiod, and hurricane disturbance, Ph.D. Dissertation, Louisiana State University, Lafayette,  
536 171 pp., 2010.
- 537 Chapin, F.S., Woodwell, G.M., Randerson, J.T., Rastetter, E.B., Lovett, G.M., Baldocchi, D.D., Clark, D.  
538 A., Harmon, M.E., Schimel, D.S., Valentini, R., Wirth, C., Aber, J.D., Cole, J.J., Goulden, M.L.,  
539 Harden, J.W., Heimann, M., Howarth, R.W., Matson, P.A., McGuire, A.D., Melillo, J.M., Mooney, H.A.,  
540 Neff, J.C., Houghton, R.A., Pace, M.L., Ryan, M.G., Running, S.W., Sala, O.E., Schlesinger, W.H.,  
541 and Schulze, E.-D.: Reconciling carbon-cycle concepts, terminology, and methods, *Ecosystems*, 9,  
542 1041-1050, doi:10.1007/s10021-005-0105-7, 2006.
- 543 Chen, B., Ge, Q., Fu, D., Yu, G., Sun, X., Wang, S., and Wang, H.: A data-model fusion approach for  
544 upscaling gross ecosystem productivity to the landscape scale based on remote sensing and flux  
545 footprint modeling, *Biogeosciences*, 7, 2943-2958, doi:10.5194/bg-7-2943-2010, 2010.
- 546 Cook, B.D., Bolstad, P.V., Martin, J.G., Heinsch, F.A. Davis, K.J., Wang, W., Desai, A.R., and Teclaw,  
547 R.M.: Using light-sue and production efficiency models to predict photosynthetic and net carbon  
548 exchange during forest canopy disturbance, *Ecosystems*, 11, 26-44, doi:10.1007/s10021-007-9105-0,  
549 2008.
- 550 Donato, D.C., Kauffman, J.B., Murdiyarso, D., Kurnianto, S., Stidham, M., and Kanninen, M.: Mangroves  
551 among the most carbon-rich forests in the tropics, *Nat. Geosci.*, 4, 293-297, doi:10.1038/ngeo1123,  
552 2011.
- 553 Gelman, A., Carlin, J.B., Stern, H.S., Rubin, D.B.: *Bayesian Data Analysis*, 2<sup>nd</sup> ed., Chapman and  
554 Hall/CRC, Boca Raton, FL., 696 pp., 2004.
- 555 Gilks, W.R., Best, N.G., and Tan, K.K.C.: Adaptive rejection metropolis sampling within Gibbs sampling,  
556 *Appl. Stat. J. Roy. St. Soc. C*, 44(4), 455-472, 1995.
- 557 Goetz, S.J., Prince, S.D., Goward, S.N., Thawley, M.M., and Small, J.: Satellite remote sensing of primary  
558 production: an improved production efficiency modeling approach, *Ecol. Model.*, 122, 239-255, 1999.
- 559 Gu, L., Baldocchi, D.D., Wofsy, S.E., Munger, J.W., Michalsky, J.J., Boden, T.A.: Response of a  
560 deciduous forest to the Mt. Pinatubo eruption: enhanced photosynthesis, *Science*, 299, 2035-2038,  
561 2003.
- 562 Heinsch F.A., Zhao, M., Running, S.W., Kimball, J. S., Nemani, R.R., Davis, K.J., Bolstad, P.V., Cook  
563 B.D., Desai, A.R., Ricciuto, D.M., Law, B.E., Oechel, W.C., Kwon, H., Luo, H., Wofsy, S.C., Dunn,  
564 A.L., Munger, J.W., Baldocchi, D.D., Xu, L., Hollinger, D.Y., Richardson, A.D., Stoy, P.C., Siqueira,  
565 M.B.S., Monson, R.K., Burns, S.P., and Flanagan, L.B.: Evaluation of remote sensing based  
566 terrestrial productivity from MODIS using regional tower eddy flux network observations, *IEEE T.*  
567 *Geosci. Remote*, 44, 1908-1925, 2006.
- 568 Huete, A., Didan, K., Miura, T., Rodriguez, E.P., Gao, X., and Ferreira, L.G.: Overview of the radiometric  
569 and biophysical performance of the MODIS vegetation indices, *Remote Sens. Environ.*, 83, 195-213,  
570 2002.
- 571 Jiang, Z., Huete, A.R., Didan, K., Miura, T.: Development of a two-band enhanced vegetation index  
572 without a blue band, *Rem. Sens. Environ.*, 112, 3833-3845, 2008.

573 Krauss, K.W., Allen, J.A.: Influences of salinity and shade on seedling photosynthesis and growth of two  
574 mangrove species, *Rhizophora mangle* and *Bruguiera sexangula*, introduced to Hawaii, *Aquat. Bot.*,  
575 77, 311-324, 2003.

576 Laffoley, D., and Grimsditch, G.: The Management of Natural Coastal Carbon Sinks, IUCN, Gland, 2009.

577 Lloyd, J., and Taylor, J.A.: On the temperature dependence of soil respiration, *Funct. Ecol.*, 8, 315-323,  
578 doi:10.2307/2389824, 1994.

579 Lovelock, C.E.: Soil respiration and belowground carbon allocation in mangrove forests, *Ecosystems*, 11,  
580 342-354, doi: 10.1007/s10021-008-9125-4, 2008.

581 Mayorga, E., Aufdenkampe, A.K., Masiello, C.A., Krusche, A.V., Hedges, J.I., Quay, P.D., Richey, J.E.,  
582 and Brown, T.A.: Young organic matter as a source of carbon dioxide outgassing from Amazonian  
583 rivers, *Nature Letters*, 436, 538-541, doi:10.1038/nature03880, 2005.

584 Monteith, J. L.: Solar radiation and productivity in tropical ecosystems, *J. Appl. Ecol.*, 9, 747-766, 1972.

585 Monteith, J. L.: The photosynthesis and transpiration of crops, *Exp. Agr.*, 2, 1-14, 1966.

586 Odum, W.E., McIvor, C.C., and Smith, T.J. III.: The ecology of the mangroves of south Florida: a  
587 community profile, U.S. Fish and Wildlife Service, Office of Biological Services, Washington, D.C.  
588 FWS/OBS-81/24. 144 pp., Reprinted September 1985., 1982.

589 O'Hagan, A. and Forster, J.J.: *Kendall's Advanced Theory of Statistics: Bayesian Inference*. 2B (2 ed.),  
590 Arnold, New York, NY, ISBN 0-340-80752-0, 2004.

591 Parida, A.K., Das, A.B., Mitra, B.: Effects of salt on growth, ion accumulation, photosynthesis and leaf  
592 anatomy of the mangrove, *Bruguiera parviflora*, *Trees*, 18, 167-174, 2004.

593 Potter, C.: The carbon budget of California, *Environ. Sci. Policy*, 13, 373-383, 2010.

594 Prince, S.D., and Goward, S.N.: Global primary production: A remote sensing approach, *J. Biogeogr.*, 22,  
595 815-835, 1995.

596 Raich, J.W., Rastetter, E.B., Melillo, J.M., Kicklighter, D.W., Steudler, P.A., Peterson, B.J., Grace, A.L.,  
597 Moore, B., and Vorosmarty, C.J.: Potential net primary productivity in South America: application of a  
598 global-model. *Ecol. Appl.*, 1(4), 399-429, 1991.

599 Reichstein, M., Falge, E., Baldocchi, D., Papale, D., Aubinet, M., Berbigier, P., Bernhofer, C., Buchmann,  
600 N., Ilmanov, T.G. Granier, A., Grunwald, T., Havrankova, K., Ilvesniemi, H., Janous, D., Knohl, A.,  
601 Laurila, T., Lohila, A., Loustau, D., Matteucci, G., Meyers, T., Miglietta, F., Ourcival, J.-M., Pumpanen,  
602 J., Rambal, S., Rotenberg, E., Sanz, M., Tenhunen, J., Seufert, G., Vaccar, F., Vesala, T., Yaki, D.,  
603 Valentini, R.: On the separation of net ecosystem exchange into assimilation and ecosystem  
604 respiration: review and improved algorithm, *Glob. Change Biol.*, 11, 1424-1439, doi:10.1111/j.1365-  
605 2486.2005.001002.x., 2005.

606 Romigh, M.M., Davis, S.E. III, Rivera-Monroy, V.H., and Twilley, R.R.: Flux of organic carbon in a riverine  
607 mangrove wetland in the Florida Coastal Everglades, *Hydrobiologia*, 569, 505-516, 2006.

608 Ross, M.S., Ruiz, P.L., Sah, J.P., and Hanan, E.J.: Chilling damage in a changing climate in coastal  
609 landscapes of the subtropical zone: a case study from south Florida, *Glob. Change Biol.*, 15, 1817-  
610 1832, doi: 10.1111/j.1365-2486.2009.01900.x, 2009.

611 Running, S.W., Baldocchi, D.D., Turner, D.P., Gower, S.T., Bakwin, P.S., and Hibbard, K.A.: A global  
612 terrestrial monitoring network integrating tower fluxes, flask sampling, ecosystem modeling and EOS  
613 satellite data. *Rem. Sens. Environ.*, 70, 108-128, 1999.

614 Running, S.W., Thornton, P.E., Nemani, R.R., and Glassy, J.M.: Global terrestrial gross and net primary  
615 productivity from the earth observing system, in: *Methods in ecosystem science*, Sala, O., Jackson,  
616 R., Mooney, H. (Eds.), Springer, New York, pp. 44-57, 2000.

617 Schubert, P., Lund, M., Ström, L., and Eklundh, L.: Impact of nutrients on peatland GPP estimations using  
618 MODIS time series data, *Rem. Sens. Environ.*, 114, 2137-2145, 2010.

619 Sobrado, M.A.: Leaf photosynthesis of the mangrove *Avicennia germinans* as affected by NaCl,  
620 *Photosynthetica*, 36(4), 547-555, 1999.

621 Souza, M.F.L., Gomes, V.R., Freitas, S.S., Andrade, R.C.B., and Knoppers, B.: Net ecosystem  
622 metabolism and nonconservative fluxes of organic matter in a tropical mangrove estuary, Piauí River  
623 (NE of Brazil), *Estuar. Coast.*, 32, 111-122, DOI 10.1007/s12237-008-9104-1, 2009.

624 Spiegelhalter, D., Thomas, A., Best N., and Lunn, D.: *WinBUGS User Manual*, Version 1.4, MRC  
625 Biostatistics Unit, Cambridge, UK., 2003.

626 Tucker, C.J., Vanpraet, C., Boerwinkel, E., Gaston, A.: Satellite remote sensing of total dry matter  
627 production in the Senegalese Sahel, *Rem. Sens. Environ.*, 13, 461-474, 1983.

628 Turner, D.P., Ritts, W.D., Cohen, W.B., Gower, S.T., Running, S.W., Zhao, M., Costa, M.H., Kirschbaum  
629 A., Ham, J., Saleska, S., and Ahl, D.: Evaluation of MODIS NPP and GPP products across multiple  
630 biomes, *Rem. Sens. Environ.*, 102, 282–292, 2006.

631 Vargas, R., Allen, M.F.: Diel patterns of soil respiration in a tropical forest after Hurricane Wilma, *J.*  
632 *Geophys. Res.*, 113, G03021, doi:10.1029/2007JG000620, 2008.

633 Xiao, X., Hollinger, D., Aber, J. D., Goltz, M., Davidson, E., Zhang, Q., and Moore III, B.: Satellite-based  
634 modeling of gross primary production in an evergreen needle leaf forest, *Rem. Sens. Environ.*, 89,  
635 519–534, 2004.

636 Zhao, M., Heinsch, F.A., Nemani, R.R., and Running, S.W.: Improvements of the MODIS terrestrial gross  
637 and net primary production global dataset, *Rem. Sens. Environ.*, 95, 164–176, 2005.

638 Zhao, M., and Running, S.W.: Remote sensing of terrestrial Primary Production and Carbon Cycle, in:  
639 *Advances in Land Remote Sensing: System, Modeling, Inversion and Application*, S. Liang (Eds.),  
640 Springer Science, pp. 423-444, 2008.

641

642

643 **Tables**

644

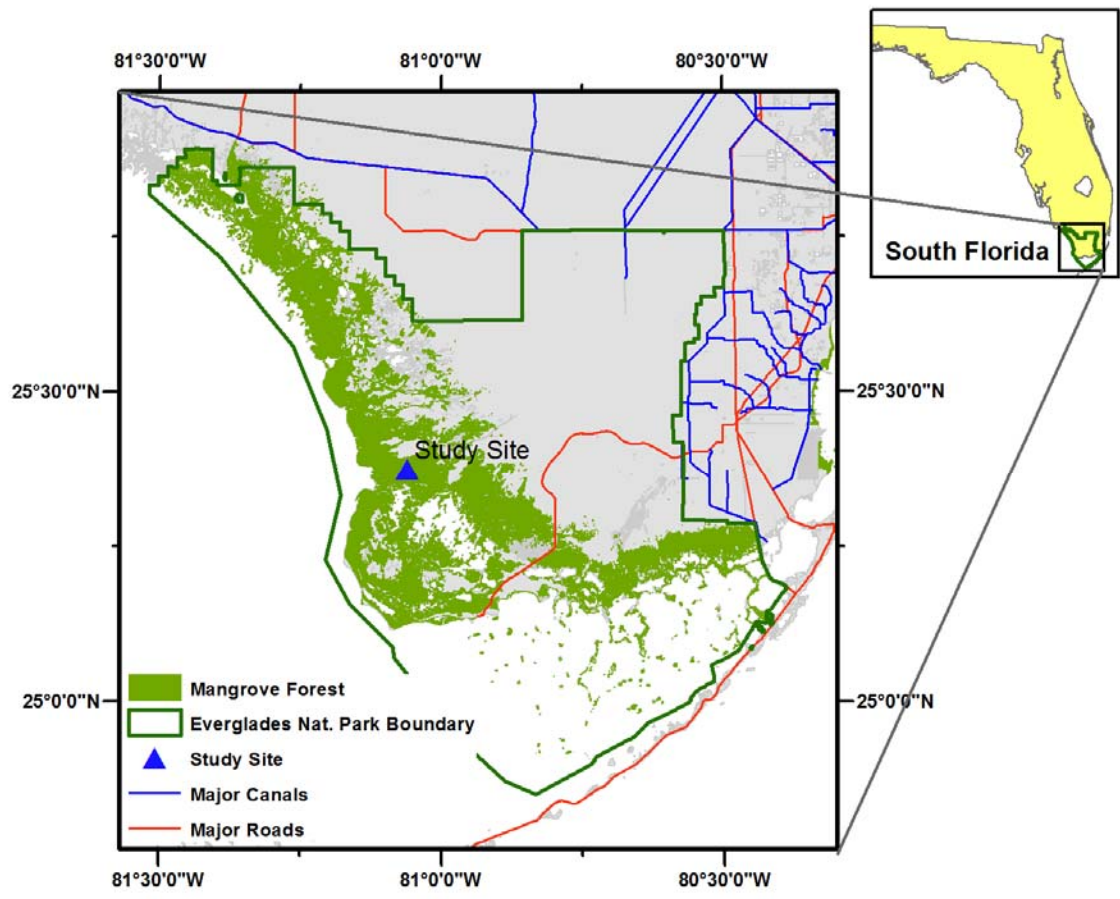
645 Table 1. MVP-LUE model forcing terms and associated uncertainty bounds

<b>Parameter</b>	<b>Description</b>	<b>Mean</b>	<b>SD</b>	<b>2.50%</b>	<b>Median</b>	<b>97.50%</b>
$\epsilon_0$	Optimum light-use efficiency (mmol C (mol photons) <sup>-1</sup> )	31.8	2.2	27.7	31.6	36.7
$m_{EVI}$	Curvature of fPAR response to EVI (dimensionless)	4.03	0.52	3.11	3.99	5.21
$T_{min}$	Temperature minimum (C)	2.6	0.6	1.4	2.7	3.7
$T_{max}$	Temperature maximum (C)	33.5	0.6	32.4	33.5	34.8
$T_{opt}$	Temperature optimum (C)	27.8	0.3	27.2	27.8	28.5
$m_{sal}$	Salinity forcing (dimensionless)	0.0047	0.0022	0.0000	0.0048	0.0084
$m_{PAR}$	PAR-saturation forcing	0.0101	0.0004	0.0092	0.0102	0.0110

646

647

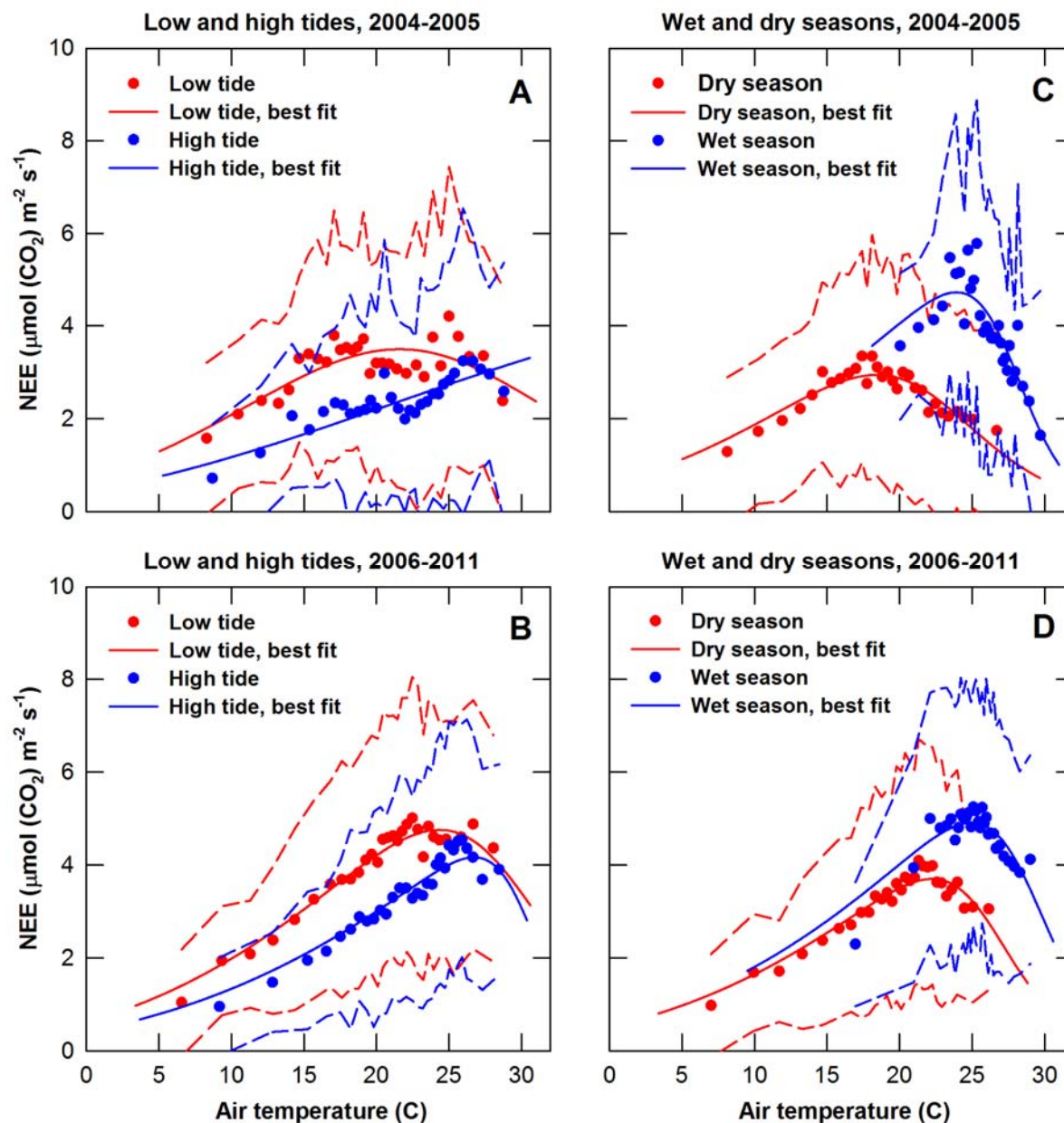
648 **Figures**  
649



650

651 Fig. 1. Map of Everglades National Park showing mangrove forest zones along the coast, the study site,  
652 and the Park boundaries, defined by the thick green line. The 30-m EC tower, SRS6, and SH3 are co-  
653 located at the study site.

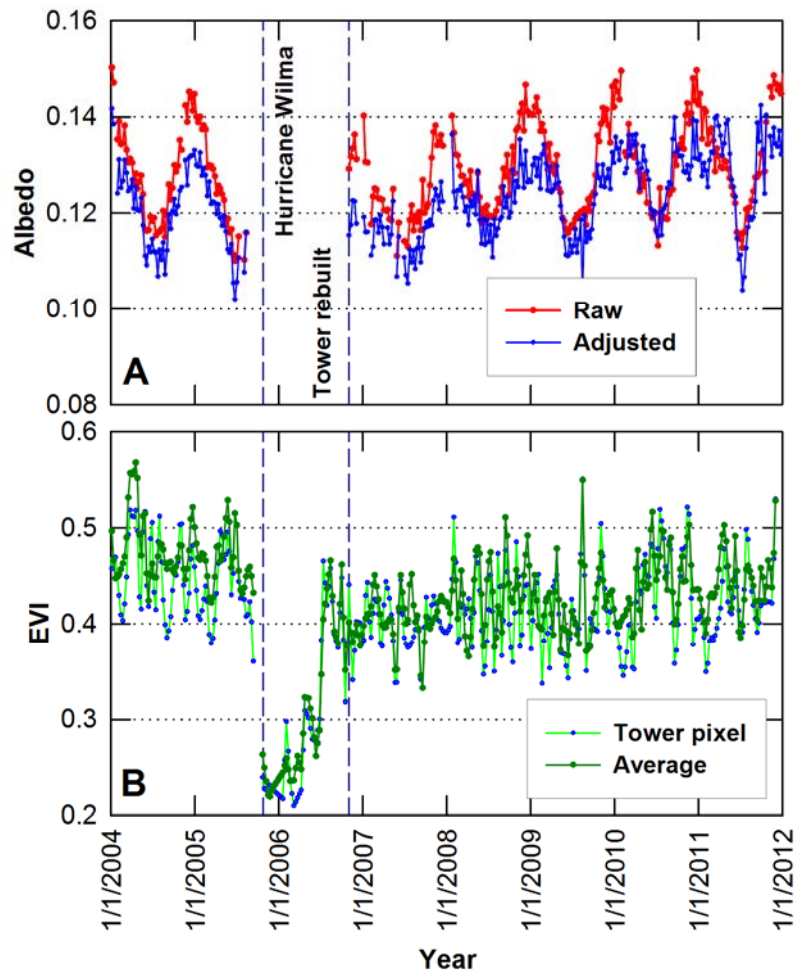
654



656

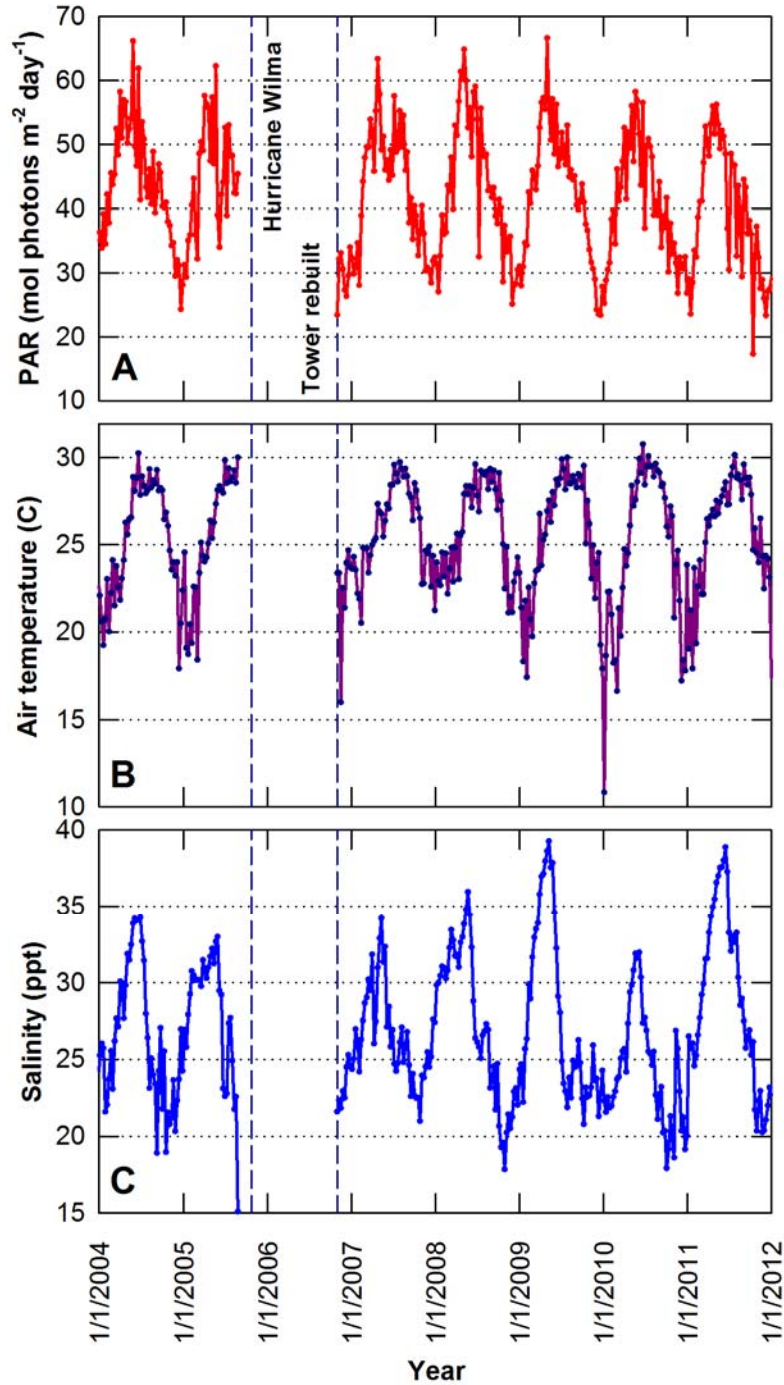
657

658 Fig. 2. Nighttime net ecosystem exchange (NEE ( $\mu\text{mol}(\text{CO}_2)\text{m}^{-2}\text{s}^{-1}$ )) versus air temperature at 27 m are  
 659 partitioned by low and high tide periods in 2004-2005 (A) and 2006-2011 (B) and by dry and wet season  
 660 months in 2004-2005 (C) and 2006-2011 (D). Each subset of the data was divided into 30 bins and the  
 661 average (circles) and  $\pm 1$  standard deviation (dashed lines) were computed for each bin. Best-fit lines  
 662 (equation 2) of the half-hourly NEE versus air temperature are included. During low tide periods, NEE is  
 663 equivalent to  $R_E$ .



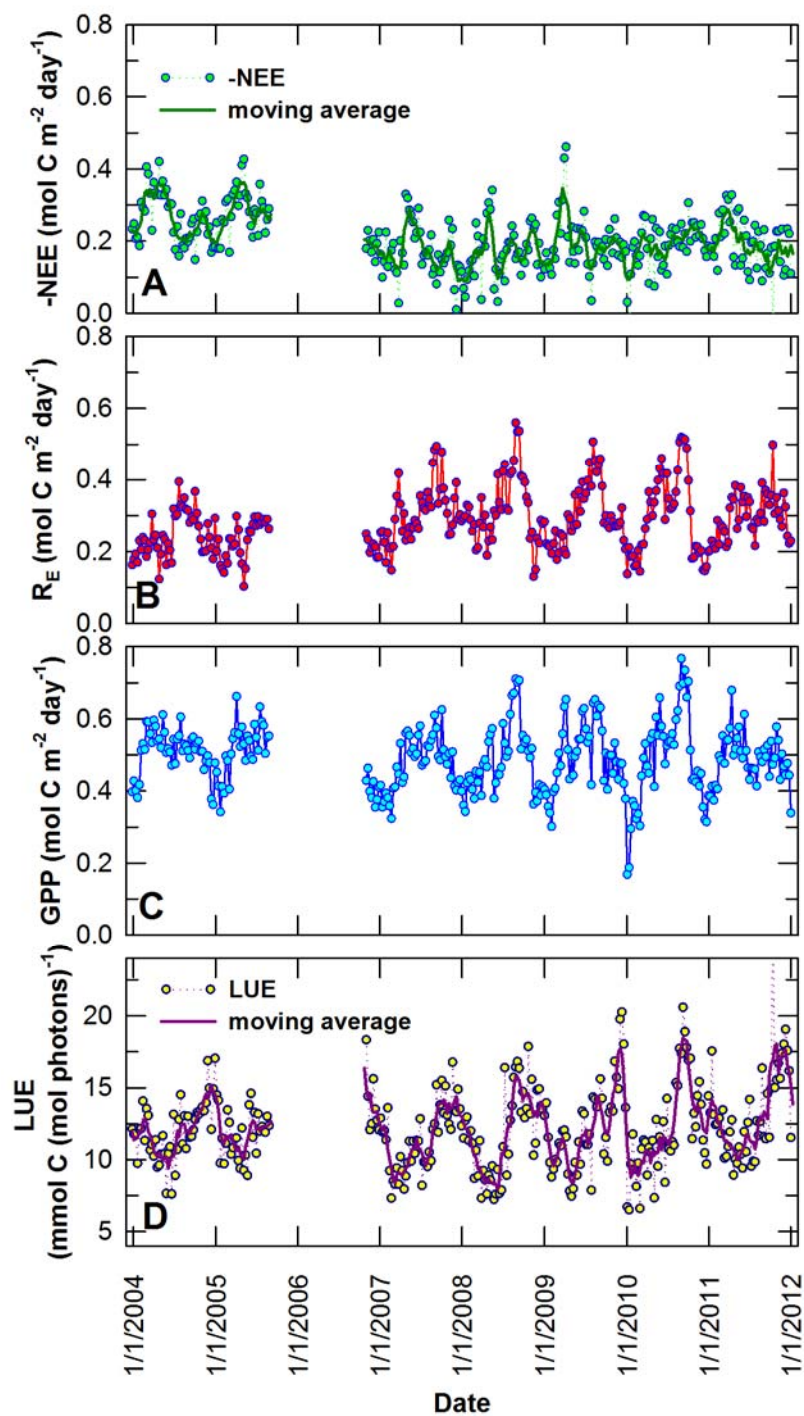
664  
 665  
 666  
 667  
 668  
 669

Fig. 3. Eight-day average albedo (raw) and albedo adjusted to include only those values when the solar elevation angle was between  $35^{\circ}$  and  $50^{\circ}$  (A). Eight-day 500-m resolution EVI (B) values were linearly interpolated using 16-day composites. Averages include the pixel that contains the tower site and the adjacent 8 pixels.



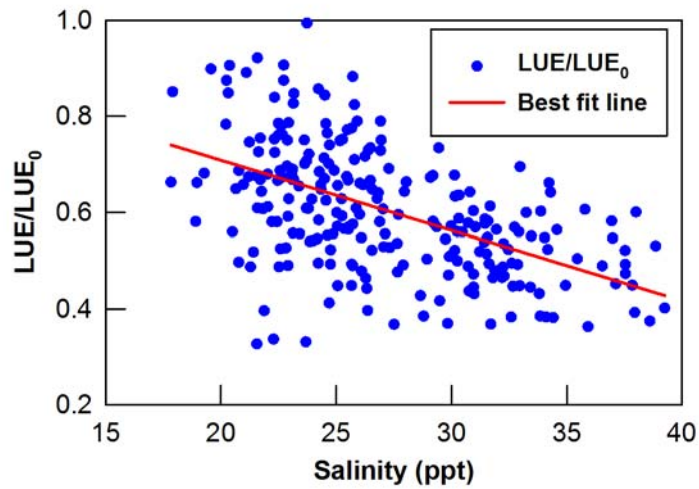
671  
 672  
 673  
 674  
 675

Fig. 4. Eight-day averages of photosynthetic active irradiance, PAR; mol (photons)  $m^{-2} day^{-1}$  (A) and air temperature ( $^{\circ}C$ ) (B) at a height of 27 m at the SRS6 tower site. Eight-day average surface water salinities (ppt) (C) measured from a well at the USGS SH3 site adjacent to the tower.



677  
678  
679  
680  
681  
682

**Fig. 5.** Eight-day sums of  $-NEE$ , mol C m<sup>-2</sup> day<sup>-1</sup> (A) from the SRS6 tower site and derived products including ecosystem respiration,  $R_E$ ; mol C m<sup>-2</sup> day<sup>-1</sup> (B), gross primary productivity,  $GPP$ ; mol C m<sup>-2</sup> day<sup>-1</sup> (C), and light (PAR) use efficiency  $LUE$ ; mmol C (mol photons)<sup>-1</sup> (D).

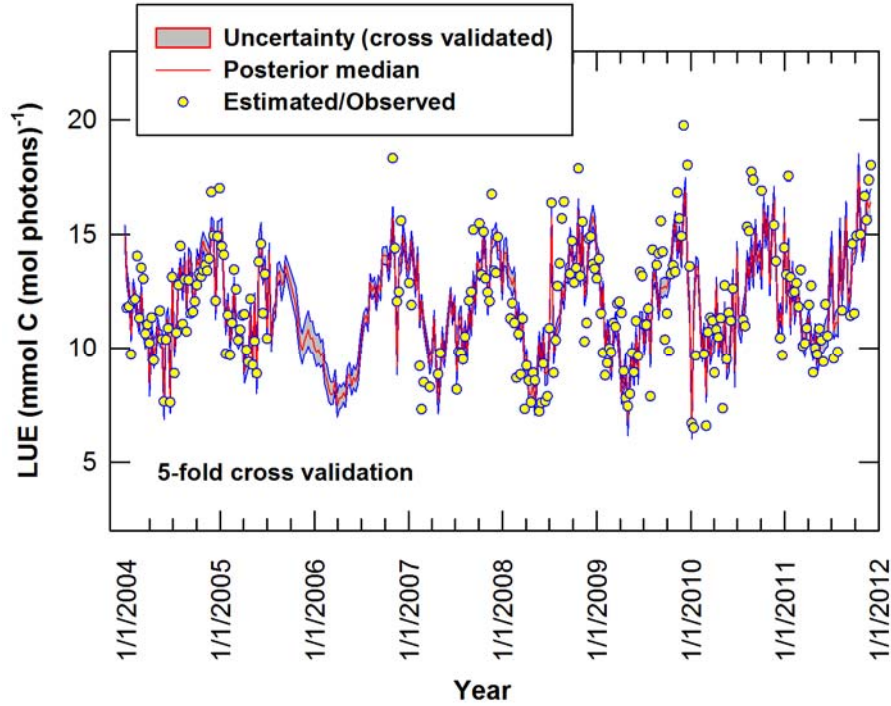


683

684 Fig. 6. Eight-day average light-use efficiency (LUE) normalized by the extrapolated LUE, LUE<sub>0</sub> at a  
685 salinity value of 0 ppt during 2004-2005 and November 2006 to December 2011. The best fit line (slope =  
686 -0.0146 and intercept = 1.0) represents the predicted decline in fractional LUE with 8-day average salinity  
687 beginning at a value of 1.0 at zero salinity.

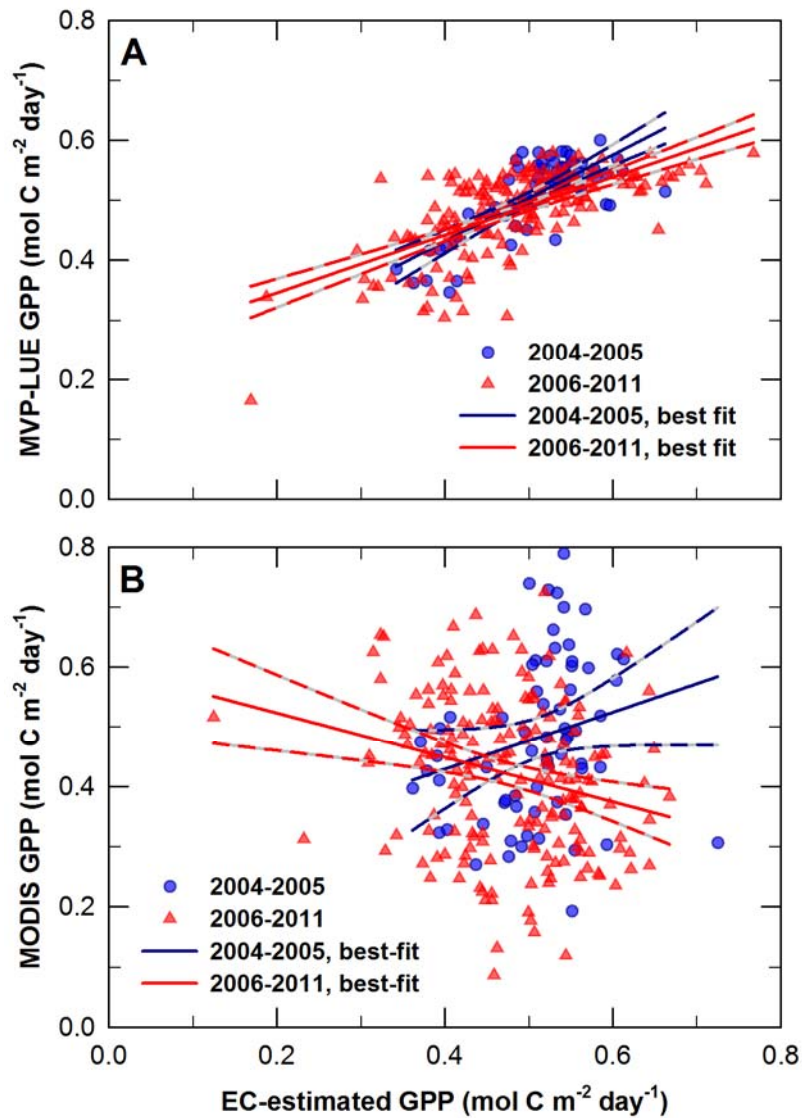
688

689



690  
 691 Fig. 7. Eight-day average estimated and modeled LUE ( $\text{mmol C (mol photons)}^{-1}$ ) at the tower site during  
 692 2004 through 2011. LUE estimates were not available from August 2005 through October 2006. The line  
 693 (red) represents the posterior median LUE and shaded area represents the 2.5% and 97.5% uncertainty  
 694 bounds. Uncertainties are provided for validation data sets derived from 5-fold cross validation. Modeled  
 695 LUE is controlled by 8-day averages of EVI, air temperature at 27 m, and surface water salinity.

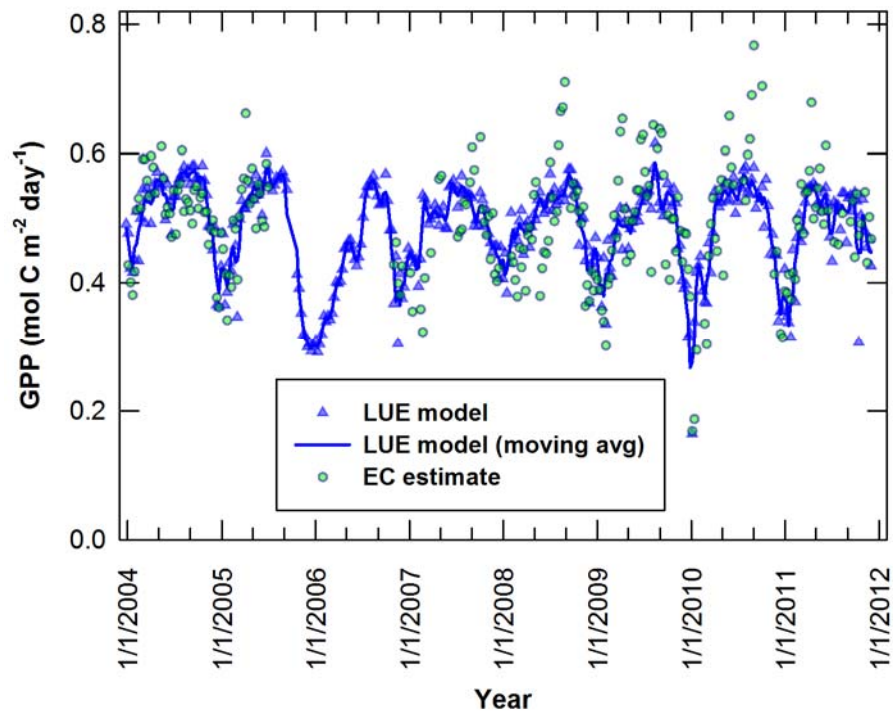
696



697

698 Fig. 8. Eight-day averages of MVP-LUE modeled GPP (LUE\*PAR) versus 8-day averages of EC-  
 699 estimated GPP during 2004-2005 and 2006-2011 (A). Best-fit lines were determined from least squares  
 700 linear regression and include 95% confidence bands for the best-fit line during 2004-2005 (slope = 0.720,  
 701 intercept = 0.144,  $R^2 = 0.56$ ) and 2006-2011 (slope = 0.483, intercept = 0.249,  $R^2 = 0.45$ ). 8-day  
 702 averages of MODIS GPP versus 8-day averages of eddy covariance estimated GPP (B) and best-fit lines  
 703 during 2004-2005 (slope = 0.477, intercept = 0.238,  $R^2 = 0.050$ ) and 2006-2011 (slope = -0.372, intercept  
 704 = 0.597,  $R^2 = 0.056$ ).

705



706

707 Fig. 9. Eight-day averages of EC-estimated and MVP-LUE modeled GPP (LUE\*PAR) and 3-period  
 708 moving average of modeled GPP during 2004-2011.

709